Laser Light-Scattering Study of the Dendritic-like Polyelectrolytes and CTAB Complex Formation

Chi Wu,*,† Rongjiu Ma,‡ Bo Zhou,‡ Jiachong Shen,‡ Kam Kwong Chan,† and Ka Fai Woo†

Department of Chemistry, The Chinese University of Hong Kong, Shatin, N.T., Hong Kong, and Department of Chemistry, Jilin University, ChangChun, China

Received August 31, 1995; Revised Manuscript Received September 29, 1995[⊗]

ABSTRACT: Dendritic-like polyelectrolytes (highly branched polymer cluster, HBNP) made from a phthalic anhydride/pentaerythritol polycondensation were investigated by laser light scattering (LLS) respectively in *N*,*N*-dimethylformamide (DMF) and buffer solutions. In DMF, individual HBNP clusters were studied and we found that they have a weight-average molar mass of 1.1×10^4 g/mol and an average hydrodynamic radius of 4.16 nm. In the buffer, the complex formation between HBNP and surfactant (cetyltrimethylammonium bromide, CTAB) was monitored by dynamic light scattering. The influence on the HBNP/CTAB complexes apparent hydrodynamic radius distribution of the HBNP:CTAB ratio, of both HBNP and CTAB concentrations, of formation time, and of pH has been examined. Our results suggested that the complex formation between HBNP and CTAB in the buffer can be modeled as the adsorption of negatively charged HBNP clusters on the cationic surface of the CTAB micelle. Further, we observed a slow aggregation of the HBNP/CTAB complexes. The stabilities of the HBNP/CTAB complex and the complex aggregates in the buffer were examined. It is found that pH can greatly influence the stabilities, which might be used in a controlled-releasing application.

Introduction

The interaction between polymer and surfactant has recently attracted much attention, mainly due to their importance in biology and colloid science. The studies of these systems lead to many important applications, such as in the flocculation of clay,[1] mineral flotation,[2] the dissolution of polymer,[3] and the recovery of crude oil.[4] It has been generally recognized that the detail of the interaction between a particular polymer and a surfactant is vitally important to the application of such a polymer/surfactant system. Among various types of polymer/surfactant systems, the interaction between linear polyelectrolytes and oppositely charged surfactants has been mostly studied.[5,6]

Models proposed for the interaction between linear polymer(s) and surfactant(s) in aqueous solution have been summarized in a recent book,[7] wherein the transfer of the hydrophobic section of a given polymer chain into a micelle was determined by the change of free energy, the balance between the hydrophobic and hydrophilic interactions. Recently, Khokhlov *et al.*[8] predicted that the interaction of a swollen polyelectrolyte gel with the oppositely charged surfactant will lead to the shrinking of the gel.

Brown *et al.*[9] recently studied the interaction between sodium poly(styrenesulfonate) (NaPSS) and CTAB. Their results showed that the NaPSS coil contracts strongly with increasing CTAB concentration, which has been attributed partially to the effect of the neutralization of the polyion charge by the oppositely charged surfactant micelles and partially to the adoption of the coil conformation to the micellar surface curvature.

In this study, we concentrated on the interaction between the dendritic-like (highly branched) polyelectrolyte cluster (HBNP) with cetyltrimethylammonium bromide (CTAB) in order to establish a model for its complex formation. One of the remarkable differences between linear polyelectrolyte chains and dendritic-like clusters is their rigidity. It is expected that the short and highly branched subchains in the cluster will be very rigid and the whole cluster will behave like a "hard sphere".

Experimental Section

Sample Preparations. The dendritic-like (highly branched) polyelectrolytes (HBNP) were prepared by a condensation of pentaerythritol and phthalic anhydride in the melt in a glycerine bath at 142 °C under vacuum for ~2 h. The initial molar ratio of pentaerythritol to phthalic anhydride was 1:2.5. The reaction's stoichiometric ratio of pentaerythritol to phthalic anhydride was 1:2. Therefore, at the end of the reaction the HBNP cluster was terminated by carboxylic groups. Before reaching its gelation threshold, the reaction vessel was immersed into ice water to stop the reaction and very sticky products were removed from the broken glass.

Cetyltrimethylammonium bromide (CTAB) from Eastman was used without further purification. The analytical grade *N*,*N*-dimethylformamide (DMF) from Riedel deHaen was purified and dried with carbon sieves before use. The dilute solution of HBNP in DMF was prepared by dissolving a proper amount of HBNP in DMF for at least 1 day to ensure complete dissolution. The solution was further clarified by a 0.1-μm Whatman filter (Anotop 25). The final solution was split into two parts: one is for laser light-scattering measurements; the other, for the specific refractive index increment (dn/dC) measurement.

The buffer (pH = 12) solution was prepared by the standard procedure (FIXAMAL Riedel deHaen). The HBNP alkaline solution was prepared by the following procedure: first, a proper amount of HBNP was dissolved in the buffer; and then, the solution was filtered into a dust-free scattering cell. The time between the addition of HBNP and the light-scattering measurement was 0.5 h. The HBNP buffer solution with the addition of CTAB was prepared in a similar way with different amounts of CTAB added after HBPN was completely dissolved in the buffer. All aqueous solutions used in this study were clarified by a Whatman PTFE filter (0.2 μm) which was wetted with methanol before use.

Laser Light Scattering (LLS). A slightly modified commercial LLS spectrometer (ALV/SP-150 equipped with an ALV-5000 multi-τ digital correlator) was used with a solid-state diode laser (ADLAS DPY425II, output power ≈ 400 mW

† Chinese University of Hong Kong.
‡ Jilin University.
[⊗] Abstract published in *Advance ACS Abstracts,* November 15, 1995.

0024-9297/96/2229-0228$12.00/0

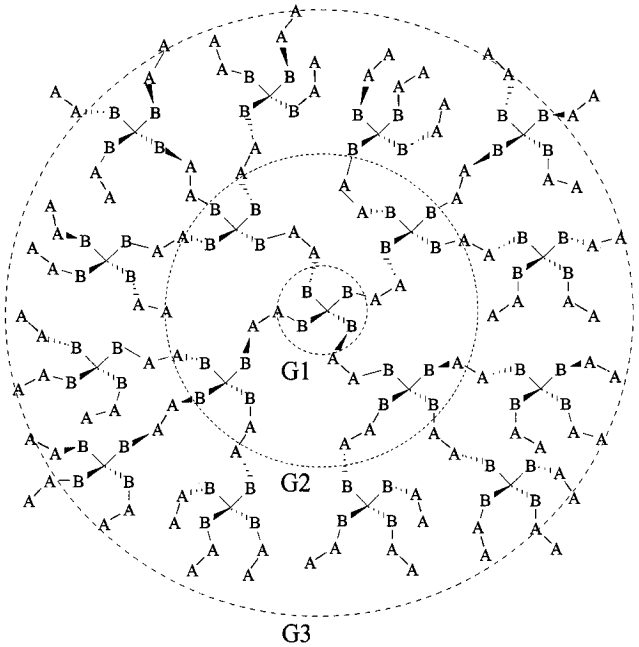

Figure 1. Schematic of the dendritic-like (highly branched) polyelectrolyte cluster (HBNP), where A and B denote the carboxylic and hydroxyl groups in phthalic anhydride and pentaerythritol, respectively. G1, G2, and G3 refer to the first, second, and third generations.

at $\lambda = 532$ nm) as the light source. The incident beam was vertically polarized with respect to the scattering plane. A compensated beam attenuator (Newport M-925B) was used to regulate the incident laser light intensity so that a possible localized heating in the light-scattering cuvette can be avoided. In static LLS, the precise dn/dC value of 0.132 ± 0.001 at $T =$ 25 °C and $\lambda = 532$ nm in DMF was determined by using a recently developed high precision differential refractometer.[10] In dynamic LLS, the intensity−intensity time correlation functions were measured. We kept the difference between the measured and calculated baselines less than 0.1%. All LLS experiments were done at 25 °C. Details of LLS experiments and instrumentation can be found elsewhere.[11]

Results and Discussion

HBNP Structure. Figure 1 shows a schematic of the dendritic-like (highly branched) polyelectrolyte cluster (HBNP, only up to three generations denoted by the dot-line circles G1, G2, and G3), where A and B represent the carboxylic and hydroxyl groups in phthalic anhydride and pentaerythritol, respectively. HBNP can dissolve in organic solvents, such as DMF. In an alkaline solution (pH ≥ 12), the surface of HBNP is anionic because −COOH changes to $-COO^-$. The hydrophilic surface enables its dissolution in the alkaline solution. In this case, HBNP is ready to adsorb other cationic molecules or particles.

Static LLS. On the basis of the LLS theory,[12,13] for a dilute macromolecule solution or colloidal suspension at concentration C (g/mL) and the scattering angle θ, the angular dependence of the excess absolute average scattered intensity, known as the excess Rayleigh ratio $[R_{vv}(\theta)]$, can be approximated as

$$\frac{KC}{R_{vv}(\theta)} \cong \frac{1}{M_w}\left(1 + \frac{1}{3}\langle R_g^2\rangle_z q^2\right) + 2A_2C \qquad (1)$$

where $K = 4\pi^2 n^2 (\partial n/\partial C)^2/(N_A\lambda_0^4)$ with N_A, n, and λ_0 being Avogadro's number, the solvent refractive index, and the wavelength of light in vacuo, respectively, and $q = (4\pi n/\lambda_0) \sin(\theta/2)$. After measuring $R_{vv}(\theta)$ at a set of C and θ, we determined the weight-average molar mass (M_w), the z-average radius of gyration ($\langle R_g^2\rangle_z^{1/2}$ or written as R_g), and the second virial coefficient (A_2) from the Zimm plot which incorporates θ and C extrapolations on a single grid.[12]

Table 1. Static and Dynamic LLS Results of the Highly Branched Polyester Nanoparticles (HBNP) in DMF at T = 25.0 °C[a]

M_W, g/mol	$10^5 A_2$, (mol·mL)/g^2	R_g, nm	$10^7\langle D\rangle$, cm^2/s	k_D, mL/g	$\langle R_h\rangle$, nm	$\mu_2/\langle D\rangle^2$
1.1×10^4	4.5		6.40	∼13	4.16	0.15

[a] The relative errors for the listed results are M_W, ±5%; A_2, ±10%; k_D, ±10%; $\langle D\rangle$, ±1%; and $\mu_2/\langle D\rangle^2$, ±10%.

Table 1 summarizes the static LLS results of HBNP in DMF at 25 °C. The positive A_2 indicates that DMF is a good solvent. No HBNP association or aggregation is expected in DMF, so that the results listed here are properties of individual HBNP clusters. The size of HBNP is too small to be accurately determined in static LLS.

Dynamic LLS. The intensity−intensity time correlation function $G^{(2)}(q,t)$ was measured, which has the form[14,15]

$$G^{(2)}(q,t) = A[1 + \beta|g^{(1)}(q,t)|^2] \qquad (2)$$

where A is a measured baseline, β ($0 \le \beta \le 1$) is a spatial coherence constant depending only on the detection optics (its value reflects the signal-to-noise ratio), and $g^{(1)}(q,t)$ is the normalized electric field (E) time correlation function. It has been shown that $g^{(1)}(q,t)$ can be related to the line-width distribution $G(\Gamma)$ by[15]

$$g^{(1)}(q,t) = \int_0^\infty G(\Gamma)\, e^{-\Gamma t}\, d\Gamma \qquad (3)$$

The Laplace inversion of eq 3 gives $G(\Gamma)$. In this study, the inversion was done by the CONTIN program[16] supplied with the ALV-5000 digital time correlator. For a diffusive relaxation, Γ is normally a function of both C and θ, which can be expressed as[17]

$$\Gamma/q^2 = D(1 + k_dC)(1 + f\langle R_g^2\rangle_z q^2) \qquad (4)$$

where k_d is the diffusion second virial coefficient and f is a dimensionless number. At $C \to 0$ and $\theta \to 0$, $\Gamma/q^2 \to D$. Therefore, with a pair of known k_d and f, we can transfer $G(\Gamma)$ obtained in a finite concentration and at a certain scattering angle into a translational diffusion coefficient distribution $G(D)$. Further, $G(D)$ can be converted into a hydrodynamic radius distribution $f(R_h)$ by using the Stokes−Einstein equation,

$$R_h = \left(\frac{k_BT}{6\pi\eta}\right)D^{-1} \qquad (5)$$

where k_B, T, and η are the Boltzmann constant, the absolute temperature, and the solvent viscosity, respectively. In the logarithmic space, $\ln(R_h) \propto \ln(D)$. For a given system, we can change $G(D)$ for the D space into the R_h space, i.e.,

$$\int_0^\infty G(D)\, dD = \int_0^\infty f(R_h)\, dR_h$$

or

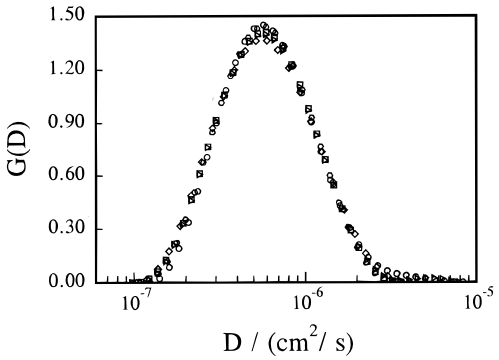

Figure 2. Angular dependence of the translational diffusion coefficient distributions ($G(D)$) of the HBNP clusters in DMF at 25 °C: (○) $\theta = 10°$; (◇) $\theta = 30°$; (△) $\theta = 60°$; (⬡) $\theta = 90°$; (□) $\theta = 150°$.

$$\int_0^\infty G(D)\, D\, \mathrm{d}[\ln(D)] = \int_0^\infty f(R_h) R_h\, \mathrm{d}[\ln(R_h)]$$

or

$$G(D)\, D \propto f(R_h)\, R_h \quad \text{or}$$

$$f(R_h) \propto \frac{G(D)\, D}{R_h} \propto G(D)\, D^2 \quad (6)$$

Since $G(\Gamma)$ is related to the scattering intensity. Thus, $f(R_h)$ defined in eq 6 is also related to the scattering intensity.

Figure 2 shows that there is virtually no angular dependence of the translational diffusion coefficient distributions ($G(D)$) for HBNP in DMF. This is expected for polymers or particles with an average hydrodynamic size smaller than 10 nm. The average translation diffusion coefficient $\langle D \rangle$, the average hydrodynamic radius $\langle R_h \rangle$, and the distribution width $\mu_2/\langle D \rangle^2$ are summarized in Table 1, where $\mu_2 = \int_0^\infty G(D)\, (D - \langle D \rangle)^2\, \mathrm{d}D$. The polydispersity index M_z/M_w estimated from $(1 + 4\mu_2/\langle D \rangle^2)$ is ~1.6, which shows that the HBNP used was moderately distributed. A single distribution peak and small hydrodynamic size further indicate that in DMF no HBNP association or aggregation exists under this condition.

The condensation between the hydroxyl group in pentaerythritol and the anhydride group in phthalic anhydride should be strictly alternating. According to its structure shown in Figure 1, a combination of static and dynamic LLS results, i.e., M_w and R_h, will enable us to very roughly estimate the average layers or generations of HBNP since we know the lengths and molecular mass of the two monomers. The estimation showed that on average HBNP has 3−4 generations with ~50 unreacted carboxylic groups on its surface.

Figure 3 shows the concentration dependence of $G(D)$ for HBNP in the buffer (pH = 12). In comparison with the distributions shown in Figure 2, there is an additional small peak which has a ~20-time smaller average $\langle D \rangle$. This small peak represents some slow diffusing (larger) species and indicates the existence of some HBNP aggregates in the buffer. Figure 3 shows that for individual HBNP the peak position is nearly independent of the HBNP concentration (C_{HBNP}). However, for the HBNP aggregates, not only the peak position shifted to a lower D, but also the peak area increased as C_{HBNP}. In the buffer, the anionic groups ($-COO^-$) on HBNP lead to its dissolution, but the rest

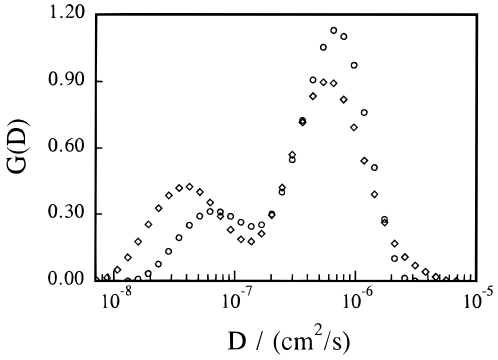

Figure 3. Concentration dependence of the translational diffusion coefficient distributions $G(D)$ of the HBNP clusters in the buffer (pH = 12): (○) $C_{HBNP} = 2$ mg/mL; (◇) $C_{HBNP} = 5$ mg/mL.

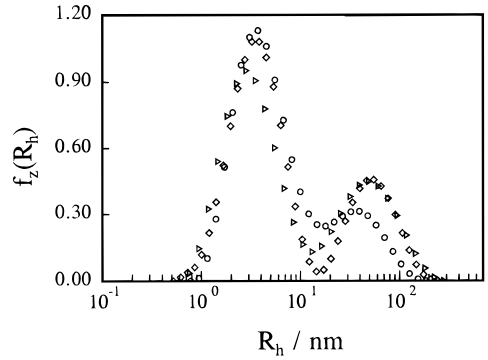

Figure 4. Time dependence of the apparent hydrodynamic radius distributions $f(R_h)$ of the HBNP clusters after its dissolution in the buffer (pH = 12): (○) $t = 1.5$ h; (◇) $t = 24$ h; (△) $t = 73.5$ h. $C_{HBNP} = 2$ mg/mL and $f(R_h)$ were calculated from $G(D)$ on the basis of eq 6.

of HBNP is still hydrophobic. There is a delicate hydrophilic and hydrophobic balance for the dissolution of HBNP in the buffer. This is why we have observed both individual HBNP clusters and HBNP aggregates.

Figure 4 shows a time dependence of the apparent hydrodynamic radius distribution $f(R_h)$ of HBNP after its dissolution in the buffer, where $C_{HBNP} = 2$ mg/mL and $f(R_h)$ were calculated from $G(D)$ on the basis of eq 6. As described above, the peak with a lower average radius (~4 nm) corresponds to individual HBNP clusters in the buffer, while the peak with a larger average size (~50 nm) is related to the HBNP aggregates. Figure 4 shows that the peak position is only slightly dependent on time, but the peak area changes as time, which indicates HBNP is not very stable in the buffer. The finite and nearly constant size of the HBNP aggregates might suggest the existence of a dynamic balance between the dissolution and aggregation processes.

Figure 5 shows a plot of the area ratio (A_L/A_S) of the two peaks in Figure 4 versus time, where the subscripts L and S refer to larger and smaller average sizes, respectively. A_L/A_S increases from its initial value of ~0.2 to a final value of ~0.6. Here, it should be noted that the area under each peak is related to the light scattered from the corresponding species (individual HBNP clusters and the HBNP aggregates). On the basis of eq 1, the scattered light intensity is proportional to both the number (n) of scatterers and the square of the scatterers' mass, i.e., $I \propto M_w \propto nM^2$. On average, the dimension of the HBNP aggregates is at least 10 times larger than that of individual HBNP clusters, which means that the mass of the HBNP aggregates is 10^2-10^3 times higher than that of individual HBNP

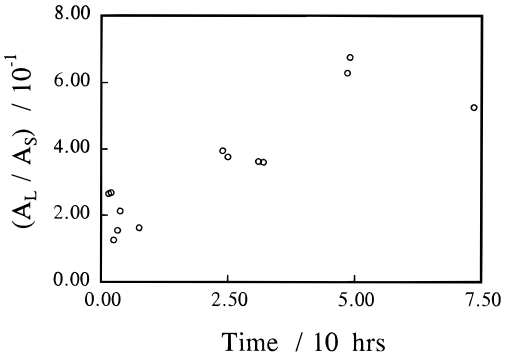

Figure 5. Time dependence of the area ratio (A_L/A_S) of the two peaks in Figure 4, where the subscripts "L" and "S" correspond to larger and smaller hydrodynamic radii, respectively.

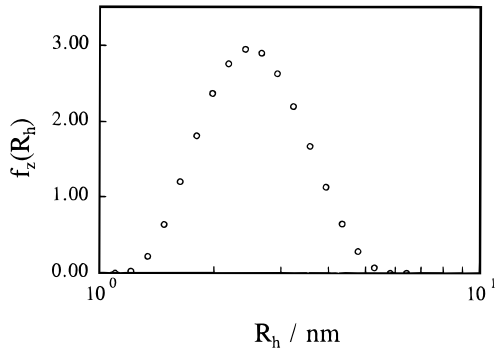

Figure 6. Typical hydrodynamic radius distribution of the CTAB micelles in the buffer (pH = 12), where C_{CTAB} = 3 mg/mL.

clusters, assuming their densities are similar. This implies that the intensity of the light scattered from one HBNP aggregate is 10^4-10^6 times higher than that from one HBNP cluster. Therefore, the actual number of the larger HBNP aggregates in the buffer is extremely small in comparison with the number of individual HBNP clusters. In other words, HBNP are individually dispersed in the buffer, except for a small number of larger HBNP aggregates.

Figure 6 shows a typical hydrodynamic radius distribution of the CTAB micelles in the buffer. It can be seen that the CTAB micelles are narrowly distributed. The average hydrodynamic radius R_{CTAB} is ~2.5 nm, which is close to the stretched length (~2.7 nm) of a single CTAB molecule. After the characterization of HBNP in both DMF and the buffer, we were ready to introduce CTAB into the HBNP buffer solution to study the complex formation between these two oppositely charged substances.

Complex Formation. Figure 7 shows a time dependence of the apparent hydrodynamic radius distribution of the HBNP/CTAB complexes after mixing HBNP and CTAB in the buffer. Initially, the distribution of the HBNP/CTAB complexes is much narrower than that of HBNP in either DMF or the buffer without adding CTAB. After standing for several days, larger aggregates gradually appeared and the size of the HBNP/CTAB complexes started to decrease.

Figure 8 shows a schematic of our proposed HBNP/CTAB complex model, wherein a number of the HBNP clusters are attracted to one CTAB micelle by electrostatic interaction. On the basis of this model, we were able to estimate the average number of the HBNP clusters attracted to each CTAB micelle from the number ratio of $N_{HBNP}/N_{micelle}$, where $N_{HBNP} = W_{HBNP}/M_{HBNP}$ and $N_{micelle} = W_{CTAB}/(a_n M_{CTAB})$ with W, M, and a_n being macroscopic weight, molar mass, and the number of CTABs in each micelle (a_n = 200−250),[18] respectively. On average, each CTAB micelle attracts ~5 HBNP clusters.

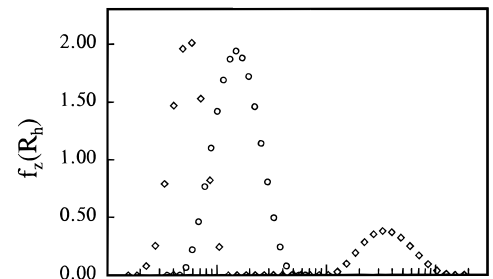

Figure 7. Time dependence of the apparent hydrodynamic radius distribution of the HBNP/CTAB complexes after mixing HBNP and CTAB in the buffer (pH = 12): (○) t = 2 h; (◇) t = 101 h. C_{HBNP} = 2 mg/mL and C_{CTAB} = 3 mg/mL.

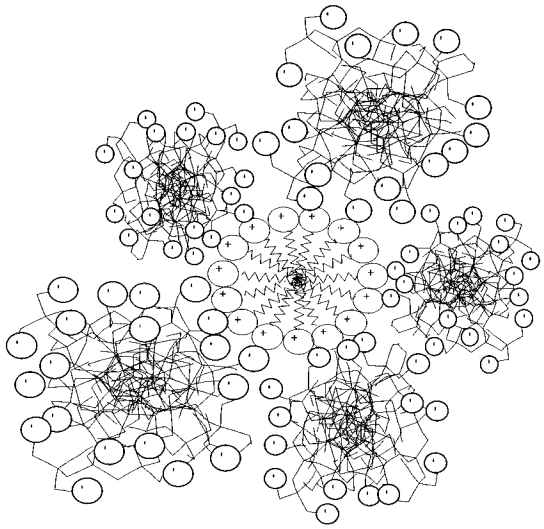

Figure 8. Schematic of the complex formation between HBNP and CTAB in the buffer (pH = 12).

In this model, the radius of the HBNP/CTAB complex is $R_{CTAB} + 2R_{HBNP}$, i.e., 11−12 nm, which is close to the observed apparent average hydrodynamic radius (~12 nm) in Figure 7. This model can also explain why the initial hydrodynamic radius distribution of the HBNP/CTAB complexes in Figure 7 is much narrower than that of the HBNP clusters in DMF because the narrowly distributed CTAB micelles act as seeds for the complex formation. Each CTAB micelle attracts a number of the HBNP clusters with different sizes, which averages the size of the formed HBNP/CTAB complexes. The long-term instability of the HBNP/CTAB complexes and further aggregation of the HBNP/CTAB complexes in the buffer might also be explained on the basis of this model, which is schematically shown in Figure 9.

Figure 10 shows, for a fixed C_{HBNP}, how the apparent hydrodynamic radius distributions of the HBNP/CTAB complexes change with increasing C_{CTAB}. It has been tested that for a fixed HBNP:CTAB ratio, the apparent size distribution depends weakly on the total concentration of HBNP and CTAB because the solution is very dilute, so that the size effect and interaction on the measured $f(R_h)$ are well separated under our conditions. The apparent size of the HBNP/CTAB complexes de-

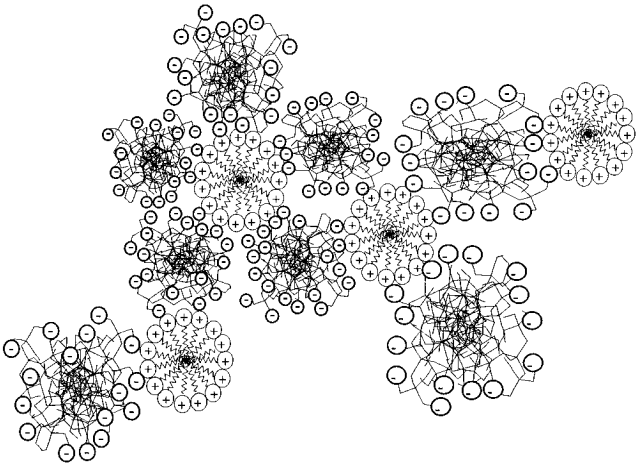

Figure 9. Schematic of the aggregation between HBNP/CTAB complexes.

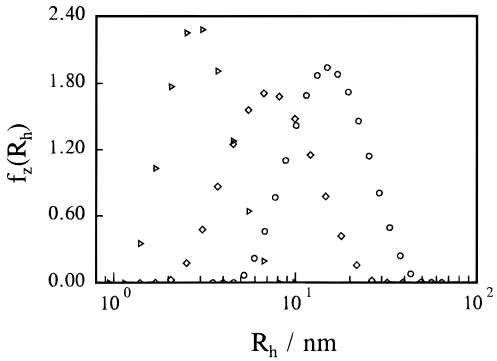

Figure 10. C_{CTAB} dependence of the apparent hydrodynamic radius distribution of the HBNP/CTAB complexes at a fixed C_{HBNP} = 2 mg/mL: (○) HBNP:CTAB = 2:3; (◇) HBNP:CTAB = 2:4; (△) HBNP:CTAB = 2:14.

creases with increasing C_{CTAB}. According to the model in Figure 8, as C_{CTAB} increases, more CTAB micelles will form in the buffer and the average number of HBNP clusters attracted to each CTAB micelle will decrease so that the apparent average size of the HBNP/CTAB complexes decreases. At higher C_{CTAB}, the formed CTAB micelles will dominate the observation. This is exactly why in Figure 10 the apparent size distribution approaches that of the CTAB micelles shown in Figure 6 when C_{CTAB} = 14 mg/mL.

Figure 11 shows the influence on the HBNP/CTAB complex stability of the pH of the buffer. At pH = 8.45, the HBNP/CTAB complexes have a finite $\langle R_h \rangle$ of ~19 nm and the complexes are stable at least within 1 week. The apparent hydrodynamic radius ($\langle R_h \rangle$) decreases much faster when the pH is higher. For each given pH, $\langle R_h \rangle$ approaches a constant value. This pH dependence property can be used in controlled-releasing applications.

Conclusion

The complex formation between dendritic-like (highly branched) polyelectrolyte clusters (HBNP) and cetyltrimethylammonium bromide (CTAB) in the buffer (pH = 12) can be modeled as the adsorption of the HBNP

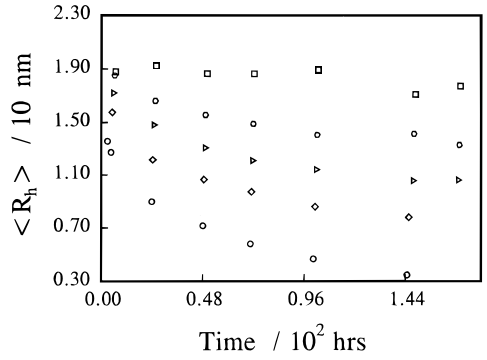

Figure 11. Time dependence of the average hydrodynamic radius ($\langle R_h \rangle$) of the HBNP/CTAB complexes in different buffers: (○) pH = 11.39; (◇) pH = 10.84; (△) pH = 10.31; (⬡) pH = 9.83; (□) pH = 8.45. C_{HBNP} = 2 mg/mL and C_{CTAB} = 3 mg/mL.

clusters on the surface of the CTAB micelle because their surfaces are oppositely charged. When the HBNP/CTAB concentration is higher, the HBNP/CTAB complexes have a tendency to form larger HBNP/CTAB complex aggregates with one or more HBNP adsorbed between two CTAB micelles. All results in this study support this model. Additional microscopic evidence is needed to justify it. Our results showed that the final size and stability of the HBNP/CTAB complexes can be controlled by pH, which will lead to controlled-release applications of this polyelectrolytes/surfactant system.

Acknowledgment. The financial support of this work by the RGC (Research Grants Council of Hong Kong Government) Earmarked Grant 1994/95 (221600260) is gratefully acknowledged.

References and Notes

(1) Hanna, H. S.; Somasundaran, P. J. *Colloid Interface Sci.* **1979**, *70*, 181.
(2) Przhegorlinskaja, R. W.; Zubkova, Yu. N. *Khim. Tuer. Topl.* **1978**, *12*, 125.
(3) Jones, M. N. J. *Colloid Interface Sci.* **1967**, *23*, 36.
(4) Taber, J. J. *Pure Appl. Chem.* **1980**, *52*, 1323.
(5) Philippova, O. E.; Karibyants, N. S.; Starodubtzev, S. G. *Macromolecules* **1994**, *27*, 2398.
(6) Philippova, O. E.; Karibyants, N. S.; Starodubtzev, S. G.; *Macromolecules* **1994**, *27*, 2398.
(7) Lindman, J.; Thalberg, K. *Interactions of Surfactants with Polymers and Proteins*; CRC Press: Boca Raton, FL, 1992; p 203.
(8) Khokhlov, A. R.; Kramarenko, E. Y.; Makhaeva, E. E. *Makromol. Chem., Theory Simul.* **1992**, *1*, 105.
(9) Fundin, J.; Brown, W. *Macromolecules* **1994**, *27*, 5024.
(10) Wu, C.; Xia, K. Q. *Rev. Sci. Instrum.* **1993**, *65*, 587.
(11) Wu, C.; Woo, K. F.; Luo, X. L.; Ma, D. Z. *Macromolecules* **1994**, *27*, 6055.
(12) Zimm, B. H. *J. Chem. Phys.* **1948**, *16*, 1099.
(13) Debye, P. *J. Phys. Colloid Chem.* **1947**, *51*, 18.
(14) Chu, B. *Laser Light Scattering*, 2nd ed.; Academic Press: New York, 1991.
(15) Berne, B.; Pecora, R. *Dynamic Light Scattering*; Plenum Press: New York, 1976.
(16) Provencher, S. W. *Biophys. J.* **1976**, *16*, 29; *J. Chem. Phys.* **1976**, *64*, 2772; *Makromol. Chem.* **1979**, *180*, 201.
(17) Stockmayer, W. H.; Schmidt, M. *Pure Appl. Chem.* **1982**, *54*, 407; *Macromolecules* **1984**, *17*, 509.
(18) Venable, R. L.; Nauman, R. V. *J. Phys. Chem.* **1964**, *68*, 3498.

MA9504429